Journal of the Korean Chemical Society
2022, *Vol. 66, No. 4*
Printed in the Republic of Korea
https://doi.org/10.5012/jkcs.2022.66.4.265

Communications

Facile and Scalable Synthetic Route to Highly Crystalline β-Sb Nanoparticles and Their Hybrids with Inorganic Nanosheets

Su Min Ahn[†], Hye Rim Kim[‡], Minju Park[†], Soyeon Yoon[†], Ayoung Yoon[†], Su-Il In[‡], and In Young Kim[*,†]

[†]*Department of Chemistry, College of Nature Sciences, Chonnam National University, Gwangju 61186, Korea.*
**E-mail: inyoung.kim@jnu.ac.kr*
[‡]*Department of Energy Science & Engineering, Daegu Gyeongbuk Institute of Science and Technology (DGIST), Daegu 42988, Korea.*

(Received June 16, 2022; Accepted July 15, 2022)

Key words: Antimony triacetate, Molybdenum sulfide, Layered double hydroxide, Hybrids, Solution-phase chemical reduction

Antimony is the semi-metal element belonging to group 15 elements of the periodic table called pnictogens. Four allotropes of antimony have been known, which are α-, β-, γ- and δ-Sb.[1] Among them, the β-Sb is the most stable allotrope in the atmosphere. Other allotropes of antimony are also quite stable in the atmosphere compared to phosphorus which is another pnictogen.[1,2] Due to high stability and semi-metallic property, the β-Sb has been applied in wide fields such as electrode materials for lithium- and sodium-ion batteries,[3,4] electrocatalysts for ammonia production,[5] and sensing materials for trace heavy metals.[6] Since reaction mechanisms in these applications include surface reactions, antimony nanostructures with large surface area are preferable to bulk antimony for superior performances in the applications.[7] In order to fabricate β-Sb, various synthetic methods have been demonstrated, which include hydrothermal and solvothermal methods,[8,9] heat-treatment,[10] high energy mechanical milling,[11] electrodeposition,[12] magnetron sputtering,[13] co-precipitation,[14] sol-gel route,[15] liquid-phase exfoliation,[16] galvanic replacement,[17] and solution-phase chemical reduction.[18] Specially, the solution-phase chemical reduction in which an antimony source is reduced by a reducing agent is a scalable, energy-saving and low-cost method as its reaction processes do not require high reaction temperature, long reaction time and expensive equipment. The most common antimony source used for the solution-phase chemical reduction is antimony trichloride[19-21] rather than antimony trioxide[22] or antimony powder. Higher solubility of antimony trichloride in water than those of antimony trioxide and antimony powder leads to complete reduction of antimony ion to antimony element without any impurities such as antimony oxychlorides and antimony trioxide. On the other hand, the use of antimony trioxide could be very harsh condition for hybridization reactions of antimony with other transition metal-based nanostructures. The antimony trichloride is readily hydrolyzed and produces hydrochloric acid with traces of water,[23] which induces decomposition of transition metal-based nanostructures such as layered double hydroxide nanosheets.[24,25] The antimony triacetate could be an alternative antimony source with small K_a for the formation of antimony nanoparticles through the solution-phase chemical reduction. To the best of our knowledge, there has been no report on facile synthetic routes to β-Sb nanoparticles and their hybrids with inorganic nanosheets using antimony triacetate as an antimony source for the solution-phase chemical reduction. Herein, facile syntheses of highly crystalline β-Sb nanoparticles and β-Sb hybrids with Zn-Cr-LDH or MoS_2 nanosheets denoted as β-Sb/Zn-Cr-LDH hybrid or β-Sb/MoS_2 hybrid are established by the solution-phase chemical reduction as illustrated in *Fig.* 1.

The synthetic procedures and characterization information for β-Sb nanoparticles, and β-Sb/MoS_2 and β-Sb/Zn-Cr-LDH hybrids are described in detail in *Supporting Information* (*SI*). Crystal structures of the samples are investigated by X-ray diffraction (XRD) analysis. As shown in *Fig.* 2, all the antimony triacetate-derived samples show XRD patterns corresponding to β-Sb without any impurity peaks. The usefulness of the antimony triacetate compared to the antimony trichloride as an antimony source is demonstrated in *SI* (*Fig.* S1 and S2).

The antimony triacetate-derived β-Sb has hexagonal crystal system with R-3m symmetry. Calculated lattice parameters of the β-Sb are a=b=4.31 Å and c=11.30 Å, while the lattice parameters of the β-Sb component in β-

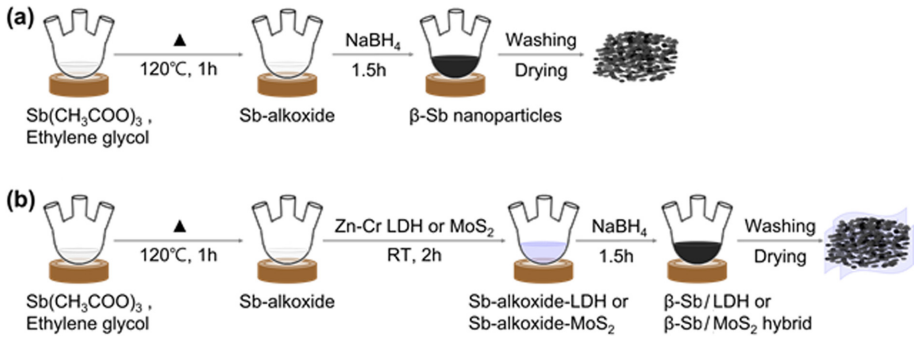

***Figure* 1.** Schematic illustration for syntheses of highly crystalline (a) β-Sb nanoparticles and (b) β-Sb/Zn-Cr-LDH or β-Sb/MoS_2 hybrids.

Sb/MoS_2 and β-Sb/Zn-Cr-LDH hybrids are determined as a=b=4.31 Å and c=11.20 Å, and a=b=4.31 Å and c=11.26 Å, respectively. It is interesting that the lattice parameters, a and b of the β-Sb retain 4.31 Å even after its hybridization with inorganic nanosheets, whereas the lattice parameter, c of the β-Sb slightly decreases upon the hybridization of the β-Sb with MoS_2 and Zn-Cr-LDH nanosheets. Considering that only the lattice parameter, c is changed for the hybrid samples, and β-Sb, MoS_2 and Zn-Cr-LDH commonly have layered crystal structures, it is inferred that the hybrid materials have a face-to-face interaction between (00l) planes of β-Sb and exfoliated nanosheets of MoS_2 or Zn-Cr-LDH.

Primary particle sizes of the samples calculated by the Scherrer equation are displayed in *Table* S1 (see *SI*). The primary particle sizes of all the samples are calculated as 36.0–51.6 nm, which vary depending on crystal-growing directions. The primary particle sizes for β-Sb component

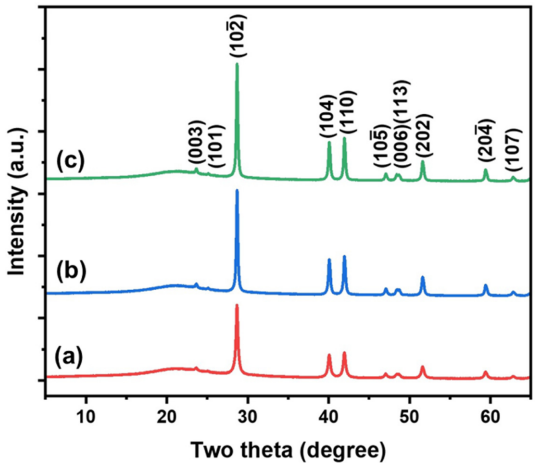

***Figure* 2.** XRD patterns of (a) β-Sb nanoparticles, and (b) β-Sb/Zn-Cr-LDH and (c) β-Sb/MoS_2 hybrids.

in β-Sb/Zn-Cr-LDH and β-Sb/MoS_2 hybrids are not significantly different compared to pure β-Sb, indicating that the hybridized inorganic nanosheets do not change a diameter of β-Sb primary particles.

A crystallinity and crystalline morphology of samples are examined by high resolution-transmission electron microscopy (HR-TEM). *Fig*. 3 shows TEM images of β-Sb nanoparticles, and β-Sb/Zn-Cr-LDH and β-Sb/MoS_2 hybrids together with those of Zn-Cr-LDH and MoS_2 nanosheets. The morphologies of Zn-Cr-LDH and MoS_2 nanosheets are anisotropic and their lateral sizes are above 200 nm (*Figs.* 3(a) and (b), respectively). The particle sizes observed by HR-TEM for pure β-Sb and β-Sb component in β-Sb/Zn-Cr-LDH and β-Sb/MoS_2 hybrids are between 30–60 nm (*Fig*. 3(c)-(f)), which is in a good agreement with the primary particle sizes calculated in *Table* S1 (see *SI*). Very importantly, as displayed in the HR-TEM image of β-Sb nanoparticles (*Fig*. 3(d)), each nanoparticle with a diameter in a range of 30–60 nm is single crystalline, demonstrating a formation of highly crystalline β-Sb nanoparticles. The co-existence of MoS_2 or Zn-Cr-LDH nanosheets with β-Sb nanoparticles is clearly confirmed in *Figs*. 3(e) and (f). The single crystalline β-Sb nanoparticles with diameters of 30–60 nm are decorated on the surface of MoS_2 or Zn-Cr-LDH nanosheets.

The homogeneous co-existence of β-Sb nanoparticles and inorganic nanosheets of Zn-Cr-LDH or MoS_2 is further cross-confirmed by field emission-scanning electron microscopy (FE-SEM) (see *Fig*. S3 in *SI*). FE-SEM analysis with energy dispersive spectroscopy (EDS) reveals that a content of β-Sb is 86at% for both β-Sb/MoS_2 and β-Sb/Zn-Cr-LDH hybrid samples (see *Fig*. S4 in *SI*).

The specific surface area of obtained samples is analyzed using the N_2 adsorption-desorption isotherms, as illustrated in *Fig*. 4. All the samples of β-Sb nanoparticles, and β-Sb/

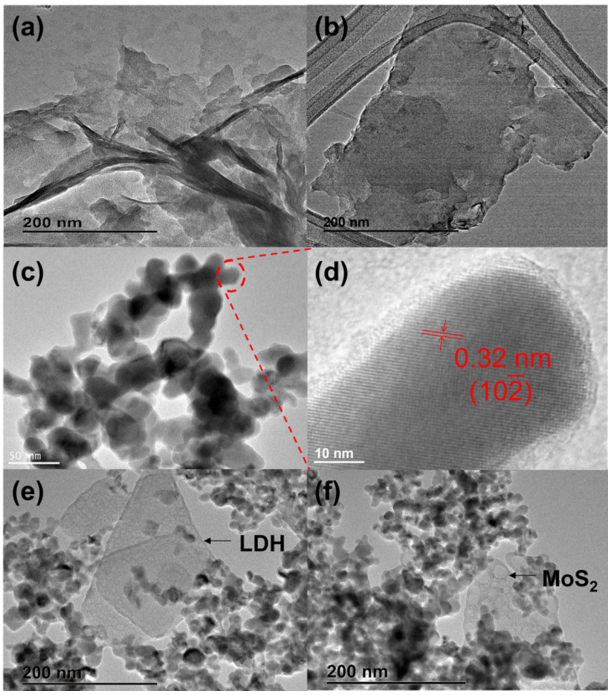

***Figure* 3.** TEM images of exfoliated (a) Zn-Cr-LDH and (b) MoS_2 nanosheets, (c,d) β-Sb nanoparticles, and (e) β-Sb/Zn-Cr-LDH and (f) β-Sb/MoS_2 hybrids.

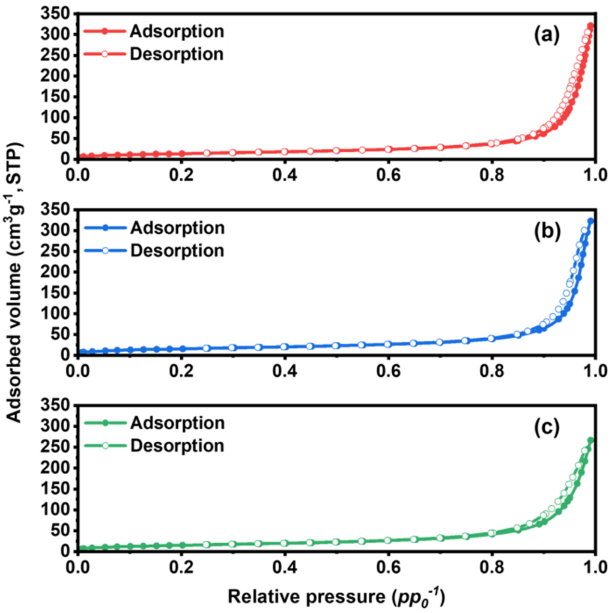

***Figure* 4.** N_2 adsorption-desorption isotherm curves of (a) β-Sb nanoparticles, and (b) β-Sb/Zn-Cr-LDH and (c) β-Sb/MoS_2 hybrids.

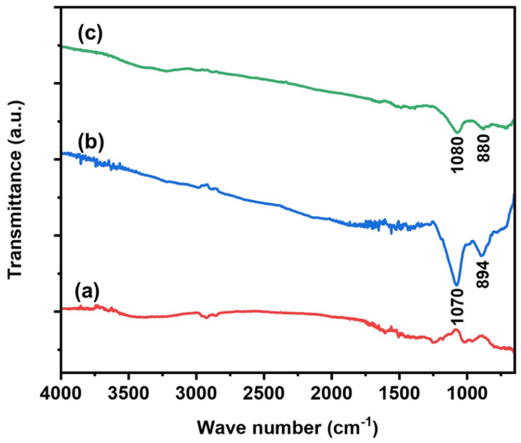

***Figure* 5.** FT-IR spectra of (a) β-Sb nanoparticles, and (b) β-Sb/Zn-Cr-LDH and (c) β-Sb/MoS_2 hybrids.

Zn-Cr-LDH and β-Sb/MoS_2 hybrids exhibit the type 4 isotherm with the H3 hysteresis loop as per the IUPAC classification, which suggests the existence of connected capillary pores.[26] Pore sizes of all the samples are in a range of 17.5–34.5 nm (see *Fig*. S5 in *SI*). The connected capillary mesopores result from interstitial space of β-Sb nanoparticles with diameters of 30–60 nm. The Brunauer-Emmett-Teller (BET) specific surface areas of β-Sb, and β-Sb/Zn-Cr-LDH and β-Sb/MoS_2 hybrids are 49.9, 58.2 and 55.3 m^2g^{-1}. The slightly expanded specific surface areas for β-Sb/Zn-Cr-LDH and β-Sb/MoS_2 hybrids are attributed to well-dispersion of β-Sb nanoparticles on the surfaces of Zn-Cr-LDH and MoS_2 nanosheets.

The chemical bond features of the samples are investigated by FT-IR analysis as presented in *Fig*. 5. The FT-IR spectrum of pure β-Sb nanoparticles shows faint FT-IR peaks, indicating a formation of alkyl ligand-free β-Sb nanoparticles. The FT-IR peaks observed at wave numbers of 880–900 cm^{-1} are stretching and bending bands of metal–oxygen or metal–sulfur bonds of β-Sb/Zn-Cr-LDH and β-Sb/MoS_2 hybrids.[27] The FT-IR bands at 1070 and 1080 cm^{-1} for β-Sb/Zn-Cr-LDH and β-Sb/MoS_2 hybrids correspond to C–N stretching bands,[27,28] which result from the uses of formamide and thiourea for the syntheses of exfoliated Zn-Cr-LDH and MoS_2 nanosheets, respectively. Considering the mild synthetic conditions and small amount of formamide and thiourea as residues, it is inferred that the formamide and thiourea are existing in interstitial space between Zn-Cr-LDH or MoS_2 nanosheets rather than functionalizing the inorganic nanosheets.

UV-Vis spectroscopic analysis is carried out to identify band structures of the β-Sb nanoparticles, and β-Sb/Zn-Cr-LDH and β-Sb/MoS_2 hybrids. As plotted in *Fig*. S6 in SI, all the samples strongly absorb light from UV to IR region (λ=185–1400 nm), suggesting metallic band structure for β-Sb nanoparticles, and β-Sb/Zn-Cr-LDH and β-Sb/MoS_2 hybrids.

In summary, we are successful in synthesizing β-Sb nanoparticles, and β-Sb/Zn-Cr-LDH and β-Sb/MoS_2 hybrids using antimony triacetate as an antimony source through solution-phase chemical reduction. The developed synthetic method is highly effective in obtaining not only high crystalline β-Sb nanoparticles but also their hybrids with inorganic nanosheets of Zn-Cr-LDH and MoS_2. High crystallinity and homogeneous particle size of β-Sb nanoparticles retain after their hybridization with Zn-Cr-LDH and MoS_2 nanosheets. The specific surface area of the β-Sb is slightly expanded upon the hybridization with the Zn-Cr-LDH and MoS_2 nanosheets. All the β-Sb nanoparticles, and β-Sb/Zn-Cr-LDH and β-Sb/MoS_2 hybrids show alkyl ligand-free chemical state and metallic properties. Considering the high crystallinity, small particle size, expanded surface area, alkyl ligand-free chemical state and high metallic properties of both hybrids, they could be promising electrode materials, and/or electrochemical catalysts in energy storage/conversion and sensing application fields.

Acknowledgments. We acknowledge Prof. Kyungsu Na and Dr. Sungho Kim for their support of this work through XRD and HR-TEM measurements, respectively. This work was supported by the National Research Foundation of Korea (NRF) grant funded by the Korea government (MSIT) (No. 2021R1C1C1008941 and No. 2021M3I3A1085039). This study was also financially supported by Chonnam National University (Grant number: 2021-2143).

Supporting Information. Experimental, XRD and SEM images for antimony trichloride-derived β-Sb/Zn-Cr-LDH hybrid, primary particle sizes, SEM images with EDS spectra and BJH pore size distribution curves.

REFERENCES

1. Wang, G.; Pandey, R.; Karna, S. P. *ACS Appl. Mater. Interfaces* **2015**, *7*, 11490.
2. Zhang, L.; Gong, T.; Yu, Z.; Dai, H.; Yang, Z.; Chen, G.; Li, J.; Pan, R.; Wang, H.; Guo, Z.; Zhang, H.; Fu, X. *Adv. Funct. Mater.* **2020**, *31*, 2005471.
3. Darwiche, A.; Marino, C.; Sougrati, M. T.; Fraisse, B.; Stievano, L.; Monconduit, L. *J. Am. Chem. Soc.* **2012**, *134*, 20805.
4. He, M.; Kravchyk, K.; Walter, M.; Kovalenko, M. V. *Nano Lett.* **2014**, *14*, 1255.
5. Jang, Y. J.; Evans, T. A.; Samanta, B.; Zeng, K.; Toroker, M.; Choi, K. -S. *J. Mater. Chem. A* **2021**, *9*, 20453.
6. Silwana, B.; Horst, C.; Iwuoha, E.; Somerset, V. *Electroanalysis* **2016**, *28*, 1597.
7. Zhang, Q; Uchaker, E.; Candelaria, S. L.; Cao, G. *Chem. Soc. Rev.* **2013**, *42*, 3127.
8. Ji, L.; Zhou, W.; Chabot, V.; Yu, A.; Xiao, X. *ACS Appl. Mater. Interfaces* **2015**, *7*, 24895.
9. Qiu, S.; Wu, X.; Xiao, L.; Ai, X.; Yang, H.; Cao, Y. *ACS Appl. Mater. Interfaces* **2016**, *8*, 1337.
10. Liu, S.; Feng, J.; Bian, X.; Liu, J.; Xu, H. *Energy Environ. Sci.* **2016**, *9*, 1229.
11. Mun, Y. S.; Yoon, Y.; Hur, J.; Park, M. S.; Bae, J.; Kim, J. H.; Yoon, Y. S.; Yoo, I. S.; Lee, S. G; Kim, I. T. *J. Power Sources* **2017**, *362*, 115.
12. Lee, C. W.; Kim, J.-C.; Park, S.; Song, H. J.; Kim, D.-W. *Nano Energy* **2015**, *15*, 479.
13. Li, Z.; Tan, X.; Li, P.; Kalisvaart, P.; Janish, M. T.; Mook, W. M.; Luber, E. J.; Jungjohann, K. L.; Carter, C. B.; Mitlin, D. *Nano Lett.* **2015**, *15*, 6339.
14. Ru, Q.; Chen, X.; Li, J.; Guo, L.; Hu, S. *Electrochim. Acta* **2015**, *177*, 304.
15. Zhou, X.; Zhong, Y.; Yang, M.; Hu, M.; Wei, J.; Zhou, Z. *Chem. Commun.* **2014**, *50*, 12888.
16. Gu, J.; Du, Z.; Zhang, C.; Ma, J.; Li, B.; Yang, S. *Adv. Energy Mater.* **2017**, *7*, 1700447.
17. Liu, J.; Yu, L.; Wu, C.; Wen, Y.; Yin, K.; Chiang, F. K.; Hu, R.; Liu, J.; Sun, L.; Gu, L.; Maier, J.; Yu, Y.; Zhu, M. *Nano Lett.* **2017**, *17*, 2034.
18. He, M.; Kravchyk, K.; Walter, M.; Kovalenko, M. V. *Nano Lett.* **2014**, *14*, 1255.
19. Dailly, A.; Ghanbaja, J.; Willmann, P.; Billaud, D. *Electrochim. Acta* **2003**, *48*, 977.
20. Zhang, P.; Wang, Y.; Wang, J.; Zhang, D.; Ren, X.; Yuan, Q. *Electrochim. Acta* **2014**, *137*, 121.
21. Yi, Y.; Shim, H.-W.; Seo, S.-D.; Dar, M. A.; Kim, D.-W. *Mater. Res. Bull.* **2016**, *76*, 338.
22. Zhou, X.; Ding, J.; Lu, H.; Qi, Z.; Yan, C. *Mater. Chem. Phys.* **2021**, *270*, 124873.
23. Hentz Jr. F.C.; Long, G. G. *J. Chem. Educ.* **1975**, *52*, 189.
24. Choy, J. H.; Kwak, S.-Y.; Jeong, Y.-J.; Park, J.-S. *Angew. Chem. Int. Ed.* **2000**, *39*, 4041.
25. Nalawade, P.; Aware, B.; Kadam, V. J.; Hirlekar, R. S. *J. Sci. Ind. Res.* **2009**, *68*, 267.
26. Sing, K. S. W.; Williams, R. T. *Adsorp. Sci. Technol.* **2004**, *22*, 773.
27. Gunjakar, J. L.; Kim, T. W.; Kim, H. N.; Kim, I. Y.; Hwang, S.-J. *J. Am. Chem. Soc.* **2011**, *133*, 14998.
28. Pavia, D. L.; Lampman, G. M.; Kriz, G. S. *Introduction to Spectroscopy*, 3rd ed.; Brooks/Cole: USA, p. 72.